

Maskless Micro/Nanopatterning and Bipolar Electrical Rectification of MoS₂ Flakes Through Femtosecond Laser Direct Writing

Pei Zuo,[†] Lan Jiang,^{†,ID} Xin Li,^{*,†,ID} Mengyao Tian,[†] Chenyang Xu,[†] Yongjiu Yuan,[†] Peng Ran,[†] Bo Li,[†] and Yongfeng Lu^{‡,ID}

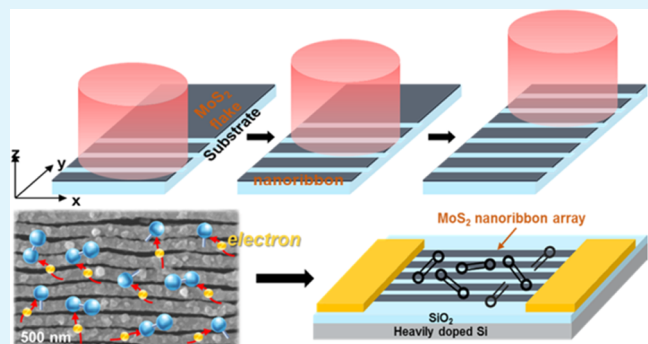
[†]Laser Micro/Nano Fabrication Laboratory, School of Mechanical Engineering, Beijing Institute of Technology, Beijing 100081, P. R. China

[‡]Laser Assisted Nano Engineering Laboratory, Department of Electrical and Computer Engineering, University of Nebraska-Lincoln, Lincoln, Nebraska 68588-0511, United States

Supporting Information

ABSTRACT: Molybdenum disulfide (MoS₂) micro/nanostructures are desirable for tuning electronic properties, developing required functionality, and improving the existing performance of multilayer MoS₂ devices. This work presents a useful method to flexibly microprocess multilayer MoS₂ flakes through femtosecond laser pulse direct writing, which can directly fabricate regular MoS₂ nanoribbon arrays with ribbon widths of 179, 152, 116, 98, and 77 nm, and arbitrarily pattern MoS₂ flakes to form micro/nanostructures such as single nanoribbon, labyrinth array, and cross structure. This method is mask-free and simple and has high flexibility, strong controllability, and high precision. Moreover, numerous oxygen molecules are chemically and physically adsorbed on laser-processed MoS₂, attributed to roughness defect sites and edges of micro/nanostructures that contain numerous unsaturated edge sites and highly active centers. In addition, electrical tests of the field-effect transistor fabricated from the prepared MoS₂ nanoribbon arrays reveal new interesting features: output and transfer characteristics exhibit a strong rectification (not going through zero and bipolar conduction) of drain–source current, which is supposedly attributed to the parallel structures with many edge defects and p-type chemical doping of oxygen molecules on MoS₂ nanoribbon arrays. This work demonstrates the ability of femtosecond laser pulses to directly induce micro/nanostructures, property changes, and new device properties of two-dimensional materials, which may enable new applications in electronic devices based on MoS₂ such as logic circuits, complementary circuits, chemical sensors, and p–n diodes.

KEYWORDS: MoS₂ flakes, femtosecond laser direct writing, micro/nanopatterning, oxygen bonding, electrical rectification



INTRODUCTION

Transition-metal dichalcogenides (TMDCs), representative layered materials like graphene, have been widely studied as a family of new-type semiconducting materials with extraordinary mechanical, electrical, optical properties, and great promise for extensive applications.^{1–6} Molybdenum disulfide (MoS₂), representative material belonging to the TMDC group, has layered structures composed of a layer of molybdenum atoms sandwiched between two layers of sulfur atoms.^{7,8} Unlike graphene with a zero band gap, MoS₂ is a band gap semiconductor with a sizable energy band gap:^{5,9} bulk MoS₂ has an indirect energy gap of ~1.2 eV and monolayer MoS₂ has a direct band gap of ~1.8 eV.³ Hence, MoS₂ can serve as a promising candidate of graphene and has excellent potential in semiconductor-related applications of layered materials such as thin-film transistors,^{1,10} integrated circuits,^{11,12} complementary inverter,¹³ photodetectors,¹⁴ light-

emitting diodes,^{15,16} photovoltaics,^{17,18} superconductors,^{19,20} and chemical/biological sensors.^{21,22}

To achieve the desired electronic properties and required functionality or improve the existing performance of MoS₂ devices, a microfabrication process is usually required to fabricate large arrays of orderly arranged MoS₂ micro/nanostructures, commonly involving patterning and etching.^{3,23} Hence, it is crucial to conduct research on MoS₂ patterning with ordered micro/nanostructures, controlled structure size, and new features for device application. Several approaches have been attempted to pattern MoS₂ materials or fabricate micro/nanostructures of MoS₂ deposited on substrates, including tape exfoliation,^{24,25} chemical vapor deposition (CVD),^{26,27} thermal decomposition of thiosalts,²⁸ van der

Received: July 24, 2019

Accepted: September 25, 2019

Published: September 25, 2019

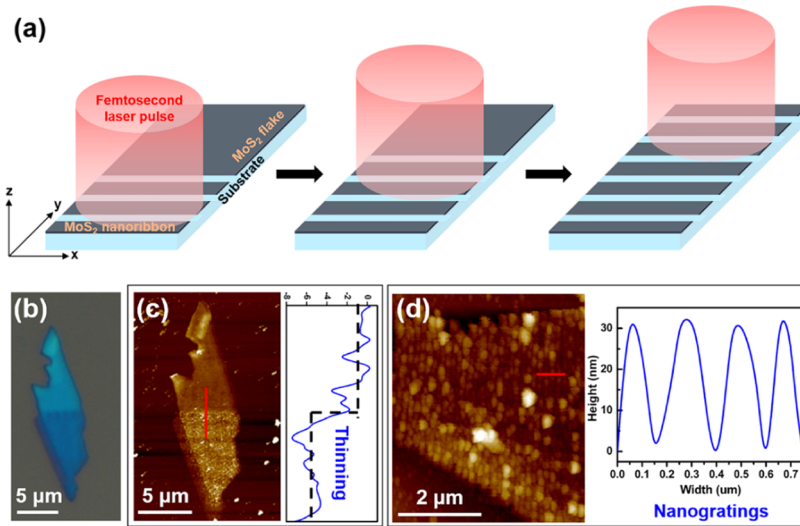


Figure 1. Principle and preliminary characterization of this method. (a) Schematic of femtosecond laser direct wiring to induce MoS₂ nanoribbons array. (b) Optical comparison of pristine MoS₂ (upper part) with FLP-MoS₂ (lower part). (c) AFM and (d) high-resolution AFM of the FLP-MoS₂ flake.

Waals epitaxial growth,^{29,30} patterned MoO₃ sulfurization,^{31,32} CVD in plasma-treated areas,^{33,34} block copolymer lithography,³⁵ reactive ion etching (RIE) combined with deposition in plasma-treated areas,³ lithography combined with stamping,²³ lithography combined with RIE,^{36,37} and continuous wave (CW) laser direct writing.^{38,39} Among them, CVD in plasma-treated areas, block copolymer lithography, lithography combined with deposition in plasma-treated areas, lithography combined with stamping, lithography combined with RIE, and CW laser direct writing can realize control for the location, shape, and size of MoS₂ micro/nanostructures. However, in the methods involving lithography, plasma surface treatment, and RIE, chemical organics (such as photoresist) and inorganic or organic masks are used, combined process are required, and the integral process is relatively complex. CW laser direct writing is a simple one-step process, needs no special atmosphere system and mask, has a relatively low cost, and has high flexibility and controllability. However, the CW laser processing is a thermal process, and the strong thermal effect would cause thermal oxidation of materials and large recasting layer, hence processing precision is insufficient. Femtosecond (ultrafast) laser pulse processing is another kind of laser processing technology.^{40,41} Femtosecond laser pulses have an ultrashort pulse width, an ultrahigh power density, and a nonlinear–nonequilibrium processing feature, and multi-photon absorption and nonthermal effects can be realized; hence, almost all the advantages of CW laser processing and femtosecond laser processing are expected as well as a high processing precision.^{42–44}

In this work, we proposed a useful method of utilizing femtosecond laser direct writing to modify the multilayer MoS₂ flakes, directly fabricate regular MoS₂ nanoribbon arrays with different ribbon widths, and arbitrarily pattern MoS₂ flakes to form different MoS₂ micro/nanostructures. Moreover, the laser-fabricated MoS₂ structures were chemically and physically bonded with numerous oxygen molecules in the air, attributed to the roughness defect sites and long edges of the nanoribbons that may contain numerous unsaturated edge sites and highly active centers. At last, electronic properties of MoS₂ nanoribbon arrays fabricated to be field-effect transistor

(FET) were tested, and the output and transfer characteristics exhibited a strong rectification (not went through zero and exhibited bipolar conduction) of drain–source current. This rectification was supposedly attributed to the parallel structures with many edge defects and p-type chemical doping of oxygen molecules on MoS₂ nanoribbon arrays, which may cause transition of n-type channel to p-type channel or properties similar to the p–n junction. The proposed method had advantages of simplicity, masklessness, strong controllability, high flexibility, and high precision and indicated the ability of femtosecond laser pulses to directly induce two-dimensional micro/nanostructures/patterns, property changes of two-dimensional material, and new device features.

RESULTS AND DISCUSSION

In this work, multilayer MoS₂ flakes were mechanically exfoliated from a natural crystal and deposited on 300 nm-SiO₂/Si substrates. The thickness of MoS₂ flakes selected for experiments was several to dozens of nanometers. Schematic of our method of fabricating MoS₂ nanoribbons/patterns is shown in Figure 1a, which is based on the formation of regular nanostructures and the material removal by femtosecond laser pulse irradiation. When focused femtosecond laser beam is irradiated on material surface, surface plasmons (SPs) of material can be induced, interference of which with incident laser field can lead to the formation of initial grating structures on material, then these initial grating structures can assist the coupling of SPs and incident laser field, leading to the further formation of final grating structures with deeper gaps.⁴⁵ The depth of gaps of laser-induced grating structures is influenced by the number and energy of ultrafast laser pulses on the unit area of material, and can be on a micrometer scale.^{42,46,47} The MoS₂ used in our experiment was a nanoscale thin flake; therefore, keeping the scan speed of laser beam slow enough (laser pulse number on unit area of MoS₂ large enough) can control the gaps penetrating the whole MoS₂ thin flake, enabling surface nanogratings to become independent nano-ribbons. Figure 1b shows the optical comparison of pristine MoS₂ with femtosecond laser-processed (FLP-) MoS₂, which showed an obvious optical color change of the MoS₂ flake after

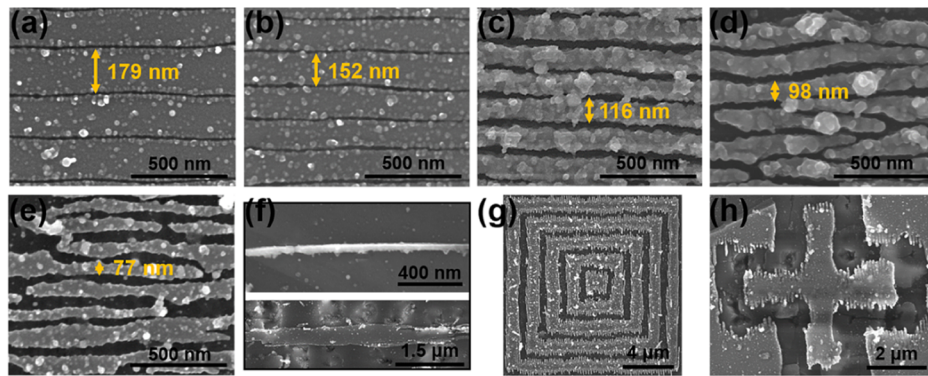


Figure 2. FLP-MoS₂ micro/nanostructures and patterns. (a–e) SEM images of regular MoS₂ nanoribbon arrays with widths of 179, 152, 116, 98, and 77 nm, respectively. (f) SEM images of two independent MoS₂ nanoribbons with widths of (above) 56 and (below) 420 nm. SEM images of (g) MoS₂ labyrinth array and (h) MoS₂ cross structure. The laser processing parameters for MoS₂ micro/nanostructures are shown in Table S1.

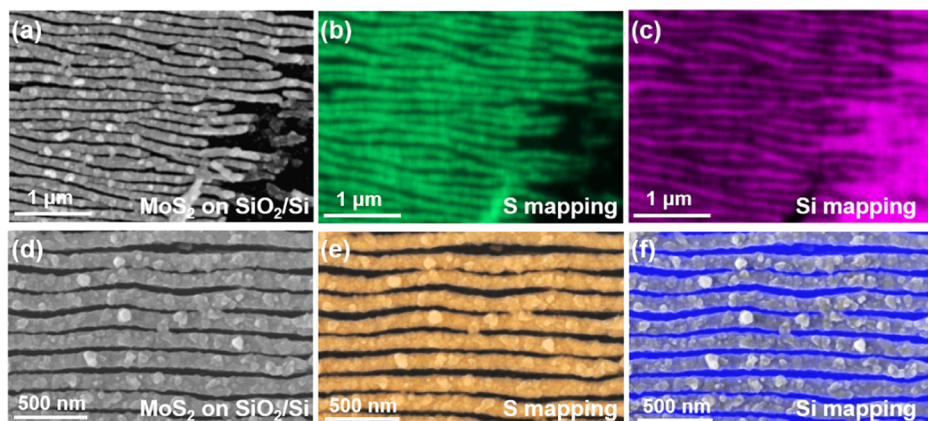


Figure 3. Formation of separated MoS₂ nanoribbons. (a) SEM image of the edge of a FLP-MoS₂ flake and its (b) S and (c) Si EDX mapping images. (d) SEM image of MoS₂ nanoribbon arrays and its (e) S and (f) Si EDX mapping images. The laser processing parameters were pulse energy of 0.015 μ J, scan interval of 0.5 μ m, and scan speed of 5 μ m/s.

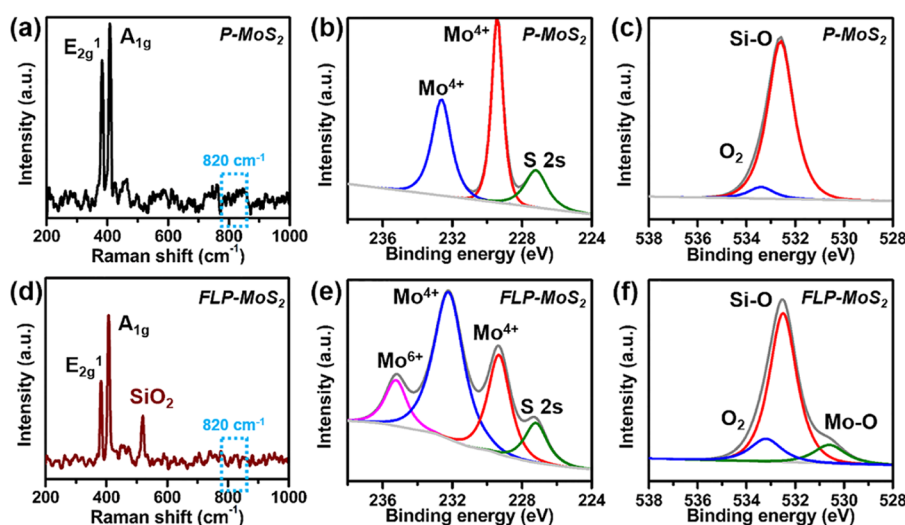


Figure 4. Raman and XPS spectra of P-MoS₂ and FLP-MoS₂. (a) Raman spectra of P-MoS₂. XPS peak-split results of (b) Mo 3d and (c) O 1s spectra of P-MoS₂. (d) Raman spectra of FLP-MoS₂, indicating no thermal oxidation for MoS₂ processed by femtosecond laser. XPS peak-split results of (e) Mo 3d and (f) O 1s spectra of FLP-MoS₂. The laser processing parameters were pulse energy of 0.015 μ J, scan interval of 0.5 μ m, and scan speed of 5 μ m/s.

142 femtosecond laser irradiation, indicating change in the
143 thickness or surface roughness. Figure 1c shows the atomic
144 force microscopy (AFM) results of the MoS₂ flake in Figure
145 1b, which indicates the reduction of the outline height of the

FLP-MoS₂ flake, suggesting a thinning effect from femtosecond laser processing on MoS₂. Figure 1d shows the high-resolution AFM image of FLP-MoS₂, which indicated the formation of MoS₂ grating structures.

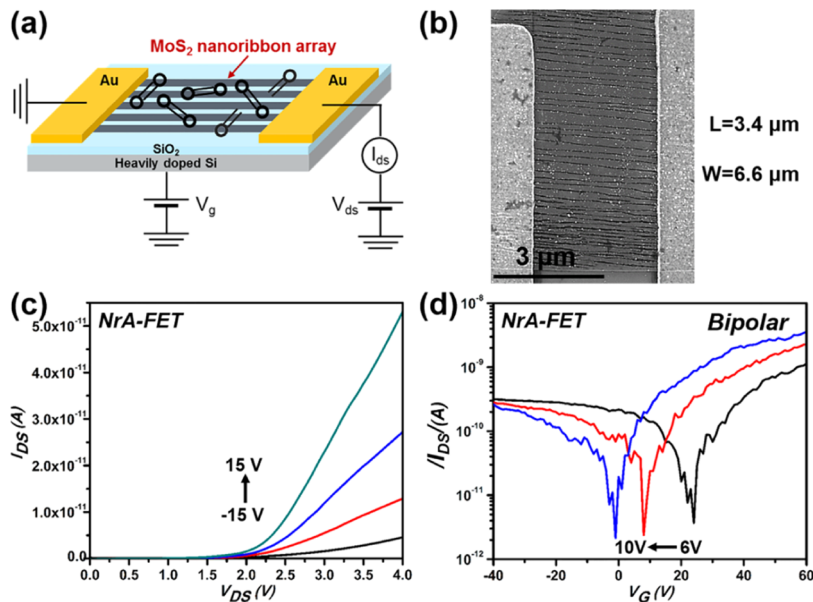


Figure 5. Electrical test of MoS₂ NrA-FET. (a) Schematic of the structure and measurement of fabricated MoS₂ NrA-FET. (b) SEM image of MoS₂ nanoribbon arrays used for fabricating FET. (c) Output and (d) transfer characteristic curve of the fabricated MoS₂ NrA-FET. The laser processing parameters for NrA are pulse energy of 0.015 μJ, scan interval of 0.5 μm, and scan speed of 10 μm/s.

To further investigate the FLP-MoS₂ micro/nanostructures, scanning electron microscopy (SEM) was carried out to characterize its physical morphology, as shown in Figure 2. Figure 2a–e shows regular MoS₂ nanoribbon arrays with different ribbon widths of approximately 179, 152, 116, 98, and 77 nm, respectively. Figure 2f shows two independent MoS₂ nanoribbons with small and big widths of 56 and 420 nm, respectively. Figure 2g,h shows two kinds of MoS₂ patterned structures obtained through material removal by femtosecond laser direct writing, which were a labyrinth array and a cross structure, indicating the flexible processing capability of femtosecond laser for arbitrary patterns. The formation of MoS₂ micro/nanostructures and the dependence of widths of nanoribbons on laser processing parameters (pulse energy and scan speed) are analyzed in the Supporting Information.

To investigate the formation of MoS₂ nanoribbons rather than surface structures on MoS₂, energy-dispersive X-ray analysis (EDX) was performed. Figure 3a–c shows the SEM images of the edge of a FLP-MoS₂ flake, and its S and Si EDX mapping images. The gray part denotes MoS₂, black part denotes the substrate, and regular striped structures were obtained through femtosecond laser processing (Figure 3a). Figure 3b shows clearly separated MoS₂ nanoribbons, and Figure 3c shows clear gaps between these MoS₂ nanoribbons. Figure 3d–f shows the SEM image of MoS₂ nanoribbon array, and its S and Si EDX mapping images, which also indicated the separation of MoS₂ nanoribbons, thus evidencing the formation of MoS₂ nanoribbons.

To investigate the change in chemical property of FLP-MoS₂ flakes, Raman and X-ray photoelectron spectroscopy (XPS) characterizations were conducted. Figure 4a–d shows the Raman spectra of pristine (P-) MoS₂ and FLP-MoS₂. There was no Raman peaks at 820 cm⁻¹ originating from MoO₃, which indicated no formation of MoO₃, thus no obvious thermal oxidation for FLP-MoS₂,⁴⁸ due to the nonthermal effect of femtosecond laser processing.⁴² No Raman peak of SiO₂ at 520 cm⁻¹ was detected on the P-MoS₂ flake; however, an obvious Raman peak of SiO₂ was detected on the FLP-

MoS₂ flake, which indicated that the substrate was also detected on the FLP-MoS₂ flake.^{49,50} This result also proved the separation of MoS₂ nanoribbons and penetrating gaps between them, consistent with the results in Figure 3. XPS Mo and O spectra of P-MoS₂ and FLP-MoS₂ are also shown in Figure 4, and their S 2p spectra are shown in Figure S8. The Mo 3d spectra of P-MoS₂ are shown in Figure 4b, which reveals three peaks (227.2, 229.3, and 232.4 eV), respectively, assigned to the S 2s orbital of the divalent sulfur, and the Mo⁴⁺ 3d_{5/2} and 3d_{3/2} orbitals of the tetravalent molybdenum.¹⁹⁷ However, in Mo 3d spectra of FLP-MoS₂ (Figure 4e), except the three peaks as shown in pristine MoS₂, there is a new peak at ~235 eV, which is assigned to the Mo⁶⁺ 3d_{3/2} orbital of the hexavalent molybdenum (calculated content of Mo⁶⁺ in all Mo is shown in Table S2). The Mo⁶⁺ in FLP-MoS₂ was attributed to the Mo–O bonds formed through the combination of oxygen with unsaturated Mo bonds, defect sites, or edge of nanoribbons that are generated from the damage and material removal of MoS₂ induced by femtosecond laser pulses.^{51,52} Figure 4c shows the O 1s spectra for P-MoS₂, which reveals two peaks (532.6 and 533.4 eV) respectively assigned to divalent oxygen from Si–O bonds and oxygen (zero valent) molecules that physically adsorbed on MoS₂ surface (O₂/MoS₂).^{53–55} The divalent oxygen from Si–O bonds came from the 300 nm SiO₂/Si substrate, and oxygen (zero valent) molecules adsorbed on the MoS₂ surface should be attributed to the intrinsic defect and edge of the flakes, which were active sites with physical adsorption capacity. However, in the O 1s spectra for FLP-MoS₂ (Figure 4f), except the strong and dominant peak assigned to divalent oxygen from Si–O bonds as shown in P-MoS₂, it revealed a stronger peak of a zero-valent oxygen of O₂/MoS₂, indicating the physical adsorption of more oxygen molecules on the MoS₂ surface; it also revealed a new peak at ~530.5 eV, which is assigned to the divalent oxygen from Mo–O bonds,^{56,57} in accordance with the result of XPS Mo 3d spectra (calculated content of O₂ and O–Mo in all O is shown in Table S2). These results indicated that more oxygen atoms/molecules were chemically and physically

combined with FLP-MoS₂. This can be attributed to the roughness surface defect sites on MoS₂ nanoribbons and long edges of nanoribbons (the defects generated by femtosecond laser ablation are elaborated in the Supporting Information), for they contained numerous unsaturated edge sites, had numerous highly active centers, and hence can physically and chemically bonded with adsorbates such as O₂ molecules (the chemical and physical reaction mechanisms of the laser-processed MoS₂ with oxygen molecules are speculated in the Supporting Information).^{58–60} The oxygen absorption on MoS₂ not only led to the change in chemical valence of MoS₂ but also, according to previous reports, can lead to p-type doping effect on MoS₂ with O₂ as an electron acceptor and MoS₂ as an electron donor (the schematic of the charge-transfer process is shown in Figure S9).⁵⁸

To evaluate the electronic properties of the prepared MoS₂ nanoribbon arrays, we fabricated a back gate FET using MoS₂ nanoribbon arrays (NrA) on SiO_{2/p} + Si substrate as a channel, with 5 nm Ti/ 75 nm Au as a source and drain electrodes, through electron beam lithography (EBL), metal evaporation deposition, and a lift-off process. The electrical measurements of fabricated FET were performed using a Keithley 4200 semiconductor characterization system in air and at room temperature. The schematic of the structure and measurement of the fabricated MoS₂ NrA-FET is shown in Figure 5a,b, where the SEM image of MoS₂ nanoribbon arrays used for fabricating FET with channel length of $L \approx 3.4 \mu\text{m}$, integral channel width of $W \approx 6.6 \mu\text{m}$, ribbon number of about 38, and gate dielectric thickness of $d = 300 \text{ nm}$ is given. For comparison, P-MoS₂ flake was also fabricated as a back-gated FET. Figure 5c shows the drain–source current (I_{DS}) versus drain–source voltage (V_{DS}) characteristics of this NrA-FET under gate voltages (V_G) ranging from -15 to 15 V. For this output characteristic curve, the drain–source current changed linearly with the drain–source voltage, indicating a nearly ohmic contact for this FET device. In addition, the output curve did not go through zero and exhibited a strong rectification of the drain–source current, which was different from the output characteristic curve of the FET fabricated using pristine/undamaged MoS₂ flake as shown in Figure S10a. This may be attributed to the parallel structures with many edge defects and p-type chemical doping of oxygen molecules on MoS₂ nanoribbon arrays, which might cause transition of n-type channel to p-type channel or properties similar to the p–n junction.^{3,61}

Figure 5d shows the drain–source current (I_{DS}) versus gate voltages (V_G) characteristics of this NrA-FET under drain–source voltage (V_{DS}) ranging from 6 to 10 V. The trend of this transfer curve was non-monotone variation and exhibited a strong rectification of the drain–source current, which was different from the transfer characteristic curve of FET fabricated using pristine/undamaged MoS₂ flake. As shown in Figure S10b, transfer characteristic curve of pristine/undamaged MoS₂ FET exhibited a n-type conduction. However, the transfer characteristic curve of MoS₂ NrA-FET exhibits a bipolar conduction, similar to the p–n type transfer conduction (Figure 5d), with current chopping by a small voltage range. To further evaluate the electronic properties of this device, on/off ratio, carrier mobility (μ), and subthreshold swing (SS) were calculated. The on/off ratio of the device was calculated to be 1.2×10^2 (p-type segment) and 1.7×10^3 (n-type segment) at the drain–source voltage (V_{DS}) of 10 V. The

carrier mobility (μ) was calculated according to equation from reported reports,²³ as shown in eq 1

$$\mu = \frac{L}{W} \frac{d}{\epsilon_0 \epsilon_r} \frac{1}{V_{DS}} \frac{\partial I_{DS}}{\partial V_G} \quad (1)$$

where L and W are length and width of the FET channel, respectively; d , ϵ_0 , and ϵ_r are thickness, vacuum permittivity, and relative permittivity of the grid dielectric layer, respectively; $\frac{\partial I_{DS}}{\partial V_G}$ can be calculated from the I_{DS} – V_G curve.

For this FET device, the length and width of the channel were $L \approx 3.4 \mu\text{m}$ and $W \approx 6.6 \mu\text{m}$, respectively; the grid dielectric layer was SiO₂, its thickness, vacuum permittivity, and relative permittivity were $d \approx 300 \text{ nm}$, $\epsilon_0 \approx 8.85 \times 10^{-12} \text{ F/m}$, and $\epsilon_r \approx 3.9 \text{ F/m}$,²³ respectively. Hence, carrier mobility of this device was calculated to be approximately $2.6 \times 10^{-3} \text{ cm}^2/\text{V}\cdot\text{s}$. The SS was calculated according to equation from previous reports,⁶² as shown in eq 2

$$\text{SS} = \frac{\Delta V_G}{\Delta \log I_{DS}} \quad (2)$$

and SS of this device was calculated to be $\sim 21 \text{ V/dec}$ according to eq 2. The obvious strong rectification behavior of I_{DS} – V_{DS} and I_{DS} – V_G of the MoS₂ NrA-FET indicated the property change of material and new device properties, which may enable new applications at electronic devices based on MoS₂ such as logic circuits, complementary circuits, chemical sensors, and p–n diodes. In addition, moderate surface modification of MoS₂ flakes by femtosecond laser pulses would also tune the n-type electronic properties of MoS₂ FET: as shown in Figure S10, the on/off ratio of MoS₂ FET was increased by two magnitude; as shown in Figure S11, the drain–source current (I_{DS}) increased quicker and reached saturation faster with the increase of gate voltages (V_G).

CONCLUSIONS

Femtosecond laser direct writing was used to nonthermally modify the multilayer MoS₂ flakes, induce separated MoS₂ nanoribbon arrays, and arbitrarily pattern MoS₂ flakes to form different MoS₂ micro/nanostructures. Optical microscopy, AFM, and SEM were performed to characterize the physical micromorphology of laser-processed MoS₂ flakes. EDX mapping indicated the separation of MoS₂ nanoribbons, proving the formation of MoS₂ nanoribbons rather than surface structures on MoS₂. Raman spectra indicated the nonthermal effect of the femtosecond laser processing, also proved the separation of MoS₂ nanoribbons and penetrating gaps between them. XPS spectra indicated that more oxygen molecules were chemically and physically bonded to FLP-MoS₂, which was attributed to the roughness defect sites on MoS₂ nanoribbons and the long edges of nanoribbons that contained numerous unsaturated edge sites and highly active centers. A MoS₂ NrA-FET was fabricated and electrical tests conducted to evaluate the electronic properties of the prepared MoS₂ nanoribbon arrays. Results indicated that output and transfer characteristic curves exhibited a strong rectification (not going through zero and bipolar conduction) of drain–source current, which were different from that of FET fabricated using pristine/undamaged MoS₂ flake. This may be attributed to the parallel structures with many edge defects and p-type chemical doping of oxygen molecules on MoS₂ nanoribbon arrays, which might cause transition of n-type

344 channel to p-type channel or properties similar to p-n
345 junction. At last, the on/off ratio, carrier mobility, and SS were
346 also calculated. The proposed method indicated the ability of
347 femtosecond laser pulses to directly induce two-dimensional
348 nanostructures and change the properties of the material and
349 new device, which may enable new applications as electronic
350 devices based on MoS₂, such as logic circuits, complementary
351 circuits, chemical sensors, and p-n diodes.

352 ■ METHODS

353 **Femtosecond Laser Processing System.** The light path setup
354 of our femtosecond laser processing system was reported in our
355 previous study.⁸ The microscope objective (50×, NA = 0.5) was used
356 to focus laser beam.

357 **Characterization of MoS₂ Nanostructures.** The optical images
358 were obtained utilizing an Olympus microscope. The AFM character-
359 ization was carried out utilizing a SPM-960 AFM. The SEM images
360 and EDX mapping spectra were obtained utilizing a Hitachi scanning
361 electron microscope. Raman spectra were obtained utilizing a
362 Renishaw InVia Reflex spectrometer (532 nm light source). XPS
363 spectra was performed utilizing a PHI Quantera X-ray photoelectron
364 spectrometer.

365 **Device Fabrication and Electrical Characterization.** Multi-
366 layer MoS₂ flakes were placed on p + Si/SiO₂ (300 nm) substrates
367 and processed by femtosecond laser pulse. Then, the substrates were
368 spin-coated with polymethyl methacrylate (PMMA) solution. The
369 source and drain electrodes were fabricated through three main steps:
370 standard electron-beam lithography (EBL) was performed by a Zeiss
371 SupraSS SEM and Raith pattern generator to pattern the PMMA
372 masks; 5 nm Ti/75 nm Au were deposited through electronic beam
373 evaporation; a lift-off process was performed in acetone. The electrical
374 measurements of the fabricated MoS₂ FET were performed using a
375 Keithley 4200 semiconductor characterization system in air and at
376 room temperature.

377 ■ ASSOCIATED CONTENT

378 ◉ Supporting Information

379 The Supporting Information is available free of charge on the
380 ACS Publications website at DOI: [10.1021/acsami.9b13059](https://doi.org/10.1021/acsami.9b13059).

381 Laser processing parameters; supplementary analysis for
382 the formation of MoS₂ micro/nanostructures; depend-
383 ence of widths of nanoribbons on laser processing
384 parameters; defects generated by femtosecond laser
385 ablation; chemical/physical reaction mechanism of laser-
386 processed MoS₂ with oxygen molecules; quantitative
387 XPS results (PDF)

388 ■ AUTHOR INFORMATION

389 Corresponding Author

390 *E-mail: lixin02@bit.edu.cn.

391 ORCID

392 Lan Jiang: [0000-0003-0488-1987](https://orcid.org/0000-0003-0488-1987)

393 Xin Li: [0000-0002-4743-5509](https://orcid.org/0000-0002-4743-5509)

394 Yongfeng Lu: [0000-0002-5942-1999](https://orcid.org/0000-0002-5942-1999)

395 Author Contributions

396 The manuscript was written through contributions of all
397 authors. All authors have given approval to the final version of
398 the manuscript.

399 Notes

400 The authors declare no competing financial interest.

■ ACKNOWLEDGMENTS

The research was supported by National Key R&D Program of China (Grant No. 2017YFB1104300), National Natural Science Foundation of China (Grant No. 51775047), and China Postdoctoral Science Foundation (Grant No. BX20190037).

■ REFERENCES

- (1) Chhowalla, M.; Jena, D.; Zhang, H. Two-dimensional semiconductors for transistors. *Nat. Rev. Mater.* **2016**, *1*, No. 16052.
- (2) Bertolazzi, S.; Bonacchi, S.; Nan, G.; Pershin, A.; Beljonne, D.; Samori, P. Engineering Chemically Active Defects in Monolayer MoS₂ Transistors via Ion-Beam Irradiation and Their Healing via Vapor Deposition of Alkanethiols. *Adv. Mater.* **2017**, *29*, No. 1606760.
- (3) Nam, H.; Wi, S.; Rokni, H.; Chen, M.; Priessnitz, G.; Lu, W.; Liang, X. MoS₂ Transistors Fabricated via Plasma-Assisted Nano-printing of Few-Layer MoS₂ Flakes into Large-Area Arrays. *ACS Nano* **2013**, *7*, 5870–5881.
- (4) Eda, G.; Maier, S. A. Two-dimensional crystals: managing light for optoelectronics. *ACS Nano* **2013**, *7*, 5660–5665.
- (5) Mak, K. F.; He, K.; Lee, C.; Lee, G. H.; Hone, J.; Heinz, T. F.; Shan, J. Tightly bound trions in monolayer MoS₂. *Nat. Mater.* **2013**, *12*, 207–211.
- (6) Yu, Y.; Ji, Z.; Zu, S.; Du, B.; Kang, Y.; Li, Z.; Zhou, Z.; Shi, K.; Fang, Z. Ultrafast Plasmonic Hot Electron Transfer in Au Nano-antenna/MoS₂ Heterostructures. *Adv. Funct. Mater.* **2016**, *26*, 6394–6401.
- (7) Behura, S.; Berry, V. interfacial nondegenerate doping of MoS₂ and other two-dimensional semiconductors. *ACS Nano* **2015**, *9*, 4227–2230.
- (8) Zuo, P.; Jiang, L.; Li, X.; Li, B.; Ran, P.; Li, X.; Qu, L.; Lu, Y. Metal (Ag, Pt)–MoS₂ Hybrids Greenly Prepared Through Photo-chemical Reduction of Femtosecond Laser Pulses for SERS and HER. *ACS Sustainable Chem. Eng.* **2018**, *6*, 7704–7714.
- (9) Lu, J.; Liu, H.; Tok, E. S.; Sow, C.-H. Interactions between lasers and two-dimensional transition metal dichalcogenides. *Chem. Soc. Rev.* **2016**, *45*, 2494–2515.
- (10) Cho, K.; Pak, J.; Kim, J.-K.; Kang, K.; Kim, T.-Y.; Shin, J.; Choi, B. Y.; Chung, S.; Lee, T. Contact-Engineered Electrical Properties of MoS₂ Field-Effect Transistors via Selectively Deposited Thiol-Molecules. *Adv. Mater.* **2018**, *30*, No. 1705540.
- (11) Cheng, R.; Jiang, S.; Chen, Y.; Liu, Y.; Weiss, N.; Cheng, H.-C.; Wu, H.; Huang, Y.; Duan, X. Few-layer molybdenum disulfide transistors and circuits for high-speed flexible electronics. *Nat. Commun.* **2014**, *5*, No. 5143.
- (12) Gao, G.; Wan, B.; Liu, X.; Sun, Q.; Yang, X.; Wang, L.; Pan, C.; Wang, Z. L. Tunable Tribotronic Dual-Gate Logic Devices Based on 2D MoS₂ and Black Phosphorus. *Adv. Mater.* **2018**, *30*, No. 1705088.
- (13) Yoo, H.; Hong, S.; On, S.; Ahn, H.; Lee, H.-K.; Hong, Y. K.; Kim, S.; Kim, J.-J. Chemical Doping Effects in Multilayer MoS₂ and Its Application in Complementary Inverter. *ACS Appl. Mater. Interfaces* **2018**, *10*, 23270–23276.
- (14) Pak, Y.; Park, W.; Mitra, S.; Sasikala Devi, A. A.; Loganathan, K.; Kumaresan, Y.; Kim, Y.; Cho, B.; Jung, G.-Y.; Hussain, M. M.; Roqan, I. S. Enhanced Performance of MoS₂ Photodetectors by Inserting an ALD-Processed TiO₂ Interlayer. *Small* **2018**, *14*, No. 1703176.
- (15) Woo, Y.; Hong, W.; Yang, S. Y.; Kim, H. J.; Cha, J.-H.; Lee, J. E.; Lee, K. J.; Kang, T.; Choi, S.-Y. Large-Area CVD-Grown MoS₂ Driver Circuit Array for Flexible Organic Light-Emitting Diode Display. *Adv. Electron. Mater.* **2018**, *4*, No. 1800251.
- (16) Choi, M.; Park, Y. J.; Sharma, B. K.; Bae, S.-R.; Kim, S. Y.; Ahn, J.-H. Flexible active-matrix organic light-emitting diode display enabled by MoS₂ thin-film transistor. *Sci. Adv.* **2018**, *4*, No. eaas8721.
- (17) Zhang, J.; Lang, X. Y.; Zhu, Y. F.; Jiang, Q. Strain tuned InSe/MoS₂ bilayer van der Waals heterostructures for photovoltaics or photocatalysis. *Phys. Chem. Chem. Phys.* **2018**, *20*, 17574–17582.

- 467 (18) Xu, M.; Chen, Y.; Xiong, F.; Wang, J.; Liu, Y.; Lv, J.; Li, Y.;
468 Wang, Y.; Chen, Z.; Ma, Y. A hidden symmetry-broken phase of MoS₂
469 revealed as a superior photovoltaic material. *J. Mater. Chem. A* **2018**,
470 *6*, 16087–16093.
- 471 (19) Chen, Q.; Lu, J.; Liang, L.; Zheliuk, O.; Ali El Yumin, A.; Ye, J.
472 Continuous Low-Bias Switching of Superconductivity in a MoS₂
473 Transistor. *Adv. Mater.* **2018**, *30*, No. 1800399.
- 474 (20) Saito, Y.; Nakamura, Y.; Bahramy, M. S.; Kohama, Y.; Ye, J.;
475 Kasahara, Y.; Nakagawa, Y.; Onga, M.; Tokunaga, M.; Nojima, T.;
476 Yanase, Y.; Iwasa, Y. Superconductivity protected by spin-valley
477 locking in ion-gated MoS₂. *Nat. Phys.* **2016**, *12*, 144.
- 478 (21) Kumar, R.; Goel, N.; Kumar, M. UV-Activated MoS₂ Based
479 Fast and Reversible NO₂ Sensor at Room Temperature. *ACS Sens.*
480 **2017**, *2*, 1744–1752.
- 481 (22) Ryu, B.; Nam, H.; Oh, B.-R.; Song, Y.; Chen, P.; Park, Y.; Wan,
482 W.; Kurabayashi, K.; Liang, X. Cyclewise Operation of Printed MoS₂
483 Transistor Biosensors for Rapid Biomolecule Quantification at
484 Femtomolar Levels. *ACS Sens.* **2017**, *2*, 274–281.
- 485 (23) Zhao, J.; Yu, H.; Chen, W.; Yang, R.; Zhu, J.; Liao, M.; Shi, D.;
486 Zhang, G. Patterned Peeling 2D MoS₂ off the Substrate. *ACS Appl.*
487 *Mater. Interfaces* **2016**, *8*, 16546–16550.
- 488 (24) Huang, M.; Li, S.; Zhang, Z.; Xiong, X.; Li, X.; Wu, Y.
489 Multifunctional high-performance van der Waals heterostructures.
490 *Nat. Nanotechnol.* **2017**, *12*, 1148.
- 491 (25) Radisavljevic, B.; Radenovic, A.; Brivio, J.; Giacometti, V.; Kis,
492 A. Single-layer MoS₂ transistors. *Nat. Nanotechnol.* **2011**, *6*, 147.
- 493 (26) Cong, R.; Qiao, S.; Liu, J.; Mi, J.; Yu, W.; Liang, B.; Fu, G.; Pan,
494 C.; Wang, S. Ultrahigh, Ultrafast, and Self-Powered Visible-Near-
495 Infrared Optical Position-Sensitive Detector Based on a CVD-
496 Prepared Vertically Standing Few-Layer MoS₂/Si Heterojunction.
497 *Adv. Sci.* **2018**, *5*, No. 1700502.
- 498 (27) Liu, H.; Zhu, Y.; Meng, Q.; Lu, X.; Kong, S.; Huang, Z.; Jiang,
499 P.; Bao, X. Role of the carrier gas flow rate in monolayer MoS₂ growth
500 by modified chemical vapor deposition. *Nano Res.* **2017**, *10*, 643–651.
- 501 (28) Liu, K.-K.; Zhang, W.; Lee, Y.-H.; Lin, Y.-C.; Chang, M.-T.; Su,
502 C.-Y.; Chang, C.-S.; Li, H.; Shi, Y.; Zhang, H.; Lai, C.-S.; Li, L.-J.
503 Growth of Large-Area and Highly Crystalline MoS₂ Thin Layers on
504 Insulating Substrates. *Nano Lett.* **2012**, *12*, 1538–1544.
- 505 (29) Pak, S.; Lee, J.; Lee, Y.-W.; Jang, A. R.; Ahn, S.; Ma, K. Y.; Cho,
506 Y.; Hong, J.; Lee, S.; Jeong, H. Y.; Im, H.; Shin, H. S.; Morris, S. M.;
507 Cha, S.; Sohn, J. I.; Kim, J. M. Strain-Mediated Interlayer Coupling
508 Effects on the Excitonic Behaviors in an Epitaxially Grown MoS₂/WS₂
509 van der Waals Heterobilayer. *Nano Lett.* **2017**, *17*, 5634–5640.
- 510 (30) Shi, Y.; Zhou, W.; Lu, A.-Y.; Fang, W.; Lee, Y.-H.; Hsu, A. L.;
511 Kim, S. M.; Kim, K. K.; Yang, H. Y.; Li, L.-J.; Idrobo, J.-C.; Kong, J.
512 van der Waals Epitaxy of MoS₂ Layers Using Graphene As Growth
513 Templates. *Nano Lett.* **2012**, *12*, 2784–2791.
- 514 (31) Xue, Y.; Zhang, Y.; Liu, Y.; Liu, H.; Song, J.; Sophia, J.; Liu, J.;
515 Xu, Z.; Xu, Q.; Wang, Z.; Zheng, J.; Liu, Y.; Li, S.; Bao, Q. Scalable
516 Production of a Few-Layer MoS₂/WS₂ Vertical Heterojunction Array
517 and Its Application for Photodetectors. *ACS Nano* **2016**, *10*, 573–
518 580.
- 519 (32) Choudhary, N.; Park, J.; Hwang, J. Y.; Chung, H.-S.; Dumas, K.
520 H.; Khondaker, S. I.; Choi, W.; Jung, Y. Centimeter Scale Patterned
521 Growth of Vertically Stacked Few Layer Only 2D MoS₂/WS₂ van der
522 Waals Heterostructure. *Sci. Rep.* **2016**, *6*, No. 25456.
- 523 (33) Chen, X.; Park, Y. J.; Das, T.; Jang, H.; Lee, J.-B.; Ahn, J.-H.
524 Lithography-free plasma-induced patterned growth of MoS₂ and its
525 heterojunction with graphene. *Nanoscale* **2016**, *8*, 15181–15188.
- 526 (34) Kim, H.-J.; Kim, H.; Yang, S.; Kwon, J.-Y. Grains in Selectively
527 Grown MoS₂ Thin Films. *Small* **2017**, *13*, No. 1702256.
- 528 (35) Han, G. G. D.; Tu, K.-H.; Niroui, F.; Xu, W.; Zhou, S.; Wang,
529 X.; Bulović, V.; Ross, C. A.; Warner, J. H.; Grossman, J. C.
530 Photoluminescent Arrays of Nanopatterned Monolayer MoS₂. *Adv.*
531 *Funct. Mater.* **2017**, *27*, No. 1703688.
- 532 (36) Jung, Y.; Shen, J.; Liu, Y.; Woods, J. M.; Sun, Y.; Cha, J. J. Metal
533 Seed Layer Thickness-Induced Transition From Vertical to
534 Horizontal Growth of MoS₂ and WS₂. *Nano Lett.* **2014**, *14*, 6842–
535 6849.
- 537 (37) Mahjouri-Samani, M.; Lin, M.-W.; Wang, K.; Lupini, A. R.; Lee, J.;
538 Basile, L.; Boulesbaa, A.; Rouleau, C. M.; Puretzky, A. A.; Ivanov, I.;
539 Xiao, K.; Yoon, M.; Geohagan, D. B. Patterned arrays of lateral
540 heterojunctions within monolayer two-dimensional semiconductors.
541 *Nat. Commun.* **2015**, *6*, No. 7749.
- 542 (38) Cao, L.; Yang, S.; Gao, W.; Liu, Z.; Gong, Y.; Ma, L.; Shi, G.;
543 Lei, S.; Zhang, Y.; Zhang, S.; Vajtai, R.; Ajayan, P. M. Direct Laser-
544 Patterned Micro-Supercapacitors from Paintable MoS₂ Films. *Small*
545 **2013**, *9*, 2905–2910.
- 546 (39) Lu, J.; Lu, J. H.; Liu, H.; Liu, B.; Chan, K. X.; Lin, J.; Chen, W.;
547 Loh, K. P.; Sow, C. H. Improved Photoelectrical Properties of MoS₂
548 Films after Laser Micromachining. *ACS Nano* **2014**, *8*, 6334–6343.
- 549 (40) Zhang, Y.; Jiao, Y.; Chen, C.; Zhu, S.; Li, C.; Li, J.; Hu, Y.; Wu,
550 D.; Chu, J. Reversible Tuning between Isotropic and Anisotropic
551 Sliding by One-Direction Mechanical Stretching on Microgrooved
552 Slippery Surfaces. *Langmuir* **2019**, *35*, 10625–10630.
- 553 (41) Wu, H.; Jiao, Y.; Zhang, C.; Chen, C.; Yang, L.; Li, J.; Ni, J.;
554 Zhang, Y.; Li, C.; Zhang, Y.; Jiang, S.; Zhu, S.; Hu, Y.; Wu, D.; Chu, J.
555 Large area metal micro-/nano-groove arrays with both structural color
556 and anisotropic wetting fabricated by one-step focused laser
557 interference lithography. *Nanoscale* **2019**, *11*, 4803–4810.
- 558 (42) Jiang, L.; Wang, A.-D.; Li, B.; Cui, T.-H.; Lu, Y.-F. Electrons
559 dynamics control by shaping femtosecond laser pulses in micro/
560 nanofabrication: modeling, method, measurement and application.
561 *Light: Sci. Appl.* **2018**, *7*, No. 17134.
- 562 (43) Wang, M.; Jiang, L.; Wang, S.; Guo, Q.; Tian, F.; Chu, Z.;
563 Zhang, J.; Li, X.; Lu, Y. Multiscale Visualization of Colloidal Particle
564 Lens Array Mediated Plasma Dynamics for Dielectric Nanoparticle
565 Enhanced Femtosecond Laser-Induced Breakdown Spectroscopy.
566 *Anal. Chem.* **2019**, *91*, 9952–9961.
- 567 (44) Jiang, S.; Hu, Y.; Wu, H.; Zhang, Y.; Zhang, Y.; Wang, Y.;
568 Zhang, Y.; Zhu, W.; Li, J.; Wu, D.; Chu, J. Multifunctional Janus
569 Microplates Arrays Actuated by Magnetic Fields for Water/Light
570 Switches and Bio-Inspired Assimilatory Coloration. *Adv. Mater.* **2019**,
571 *31*, No. 1807507.
- 572 (45) Huang, M.; Zhao, F.; Cheng, Y.; Xu, N.; Xu, Z. Origin of Laser-
573 Induced Near-Subwavelength Ripples: Interference between Surface
574 Plasmons and Incident Laser. *ACS Nano* **2009**, *3*, 4062–4070.
- 575 (46) Shuangshuang, H.; Yanyan, H.; Pingxin, X.; Yi, Z.; Shian, Z.;
576 Tianqing, J.; Zhenrong, S.; Jianrong, Q.; Zhizhan, X. Formation of
577 long- and short-periodic nanoripples on stainless steel irradiated by
578 femtosecond laser pulses. *J. Phys. D: Appl. Phys.* **2011**, *44*,
579 No. 505401.
- 580 (47) Xia, B.; Jiang, L.; Li, X.; Yan, X.; Zhao, W.; Lu, Y. High aspect
581 ratio, high-quality microholes in PMMA: a comparison between
582 femtosecond laser drilling in air and in vacuum. *Appl. Phys. A* **2015**,
583 *119*, 61–68.
- 584 (48) Paradisanos, I.; Kymakis, E.; Fotakis, C.; Kiouoglou, G.;
585 Stratidakis, E. Intense femtosecond photoexcitation of bulk and
586 monolayer MoS₂. *Appl. Phys. Lett.* **2014**, *105*, No. 041108.
- 587 (49) Serincan, U.; Kartopu, G.; Guennes, A.; Finstad, T. G.; Turan,
588 R.; Ekinci, Y.; Bayliss, S. C. Characterization of Ge nanocrystals
589 embedded in SiO₂ by Raman spectroscopy. *Semicond. Sci. Technol.* **2004**,
590 *19*, 247.
- 591 (50) Nesheva, D.; Raptis, C.; Perakis, A.; et al. Raman scattering and
592 photoluminescence from Si nanoparticles in annealed SiOx thin films.
593 *J. Appl. Phys.* **2002**, *92*, 4678–4683.
- 594 (51) Wei, X.; Yu, Z.; Hu, F.; Cheng, Y.; Yu, L.; Wang, X.; Xiao, M.;
595 Wang, J.; Wang, X.; Shi, Y. Mo-O bond doping and related-defect
596 assisted enhancement of photoluminescence in monolayer MoS₂. *AIP*
597 *Adv.* **2014**, *4*, No. 123004.
- 598 (52) da Silveira Firmiano, E. G.; Rabelo, A. C.; Dalmaschio, C. J.;
599 Pinheiro, A. N.; Pereira, E. C.; Schreiner, W. H.; Leite, E. R.
600 Supercapacitor electrodes obtained by directly bonding 2D MoS₂ on
601 reduced graphene oxide. *Adv. Energy Mater.* **2014**, *4*, No. 1301380.
- 602 (53) Hollinger, G. Structures chimique et electronique de l'interface
603 SiO₂-Si. *Appl. Surf. Sci.* **1981**, *8*, 318–336.

- 603 (54) Shuxian, Z.; Hall, W. K.; Ertl, G.; Knözinger, H. X-ray
604 photoemission study of oxygen and nitric oxide adsorption on MoS₂.
605 *J. Catal.* **1986**, *100*, 167–175.
606 (55) Finster, J.; Klinkenberg, E.-D.; Heeg, J.; Braun, W. ESCA and
607 SEXAFS investigations of insulating materials for ULSI micro-
608 electronics. *Vacuum* **1990**, *41*, 1586–1589.
609 (56) Colton, R. J.; Guzman, A. M.; Rabalais, J. W. Electrochromism
610 in some thin-film transition-metal oxides characterized by x-ray
611 electron spectroscopy. *J. Appl. Phys.* **1978**, *49*, 409–416.
612 (57) Chowdari, B.; Tan, K.; Chia, W.; Gopalakrishnan, R. X-ray
613 photoelectron spectroscopic studies of molybdenum phosphate glassy
614 system. *J. Non-Cryst. Solids* **1990**, *119*, 95–102.
615 (58) Nan, H.; Wang, Z.; Wang, W.; Liang, Z.; Lu, Y.; Chen, Q.; He,
616 D.; Tan, P.; Miao, F.; Wang, X.; Wang, J.; Ni, Z. Strong
617 Photoluminescence Enhancement of MoS₂ through Defect Engineer-
618 ing and Oxygen Bonding. *ACS Nano* **2014**, *8*, 5738–5745.
619 (59) Zhou, W.; Zou, X.; Najmaei, S.; Liu, Z.; Shi, Y.; Kong, J.; Lou,
620 J.; Ajayan, P. M.; Yakobson, B. I.; Idrobo, J.-C. Intrinsic structural
621 defects in monolayer molybdenum disulfide. *Nano Lett.* **2013**, *13*,
622 2615–2622.
623 (60) Yan, Y.; Xia, B.; Ge, X.; Liu, Z.; Wang, J.-Y.; Wang, X. Ultrathin
624 MoS₂ nanoplates with rich active sites as highly efficient catalyst for
625 hydrogen evolution. *ACS Appl. Mater. Interfaces* **2013**, *5*, 12794–
626 12798.
627 (61) Tang, Q.; Tong, Y.; Li, H.; Ji, Z.; Li, L.; Hu, W.; Liu, Y.; Zhu,
628 D. High-Performance Air-Stable Bipolar Field-Effect Transistors of
629 Organic Single-Crystalline Ribbons with an Air-Gap Dielectric. *Adv.
630 Mater.* **2008**, *20*, 1511–1515.
631 (62) Wang, X.; Zhang, T.-B.; Yang, W.; Zhu, H.; Chen, L.; Sun, Q.-
632 Q.; Zhang, D. W. Improved integration of ultra-thin high-k dielectrics
633 in few-layer MoS₂ FET by remote forming gas plasma pretreatment.
634 *Appl. Phys. Lett.* **2017**, *110*, No. 053110.